

PAPER

Phase transitions and crystal-field and exchange interactions in $\text{TbFe}_3(\text{BO}_3)_4$ as seen via optical spectroscopy

To cite this article: M N Popova *et al* 2012 *J. Phys.: Condens. Matter* **24** 196002

View the [article online](#) for updates and enhancements.

Related content

- [Magnetic and specific heat properties of \$\text{YFe}_3\(\text{BO}_3\)_4\$ and \$\text{ErFe}_3\(\text{BO}_3\)_4\$](#)
E A Popova, A N Vasiliev, V L Temerov *et al.*
- [Magnetic structure in iron borates \$\text{RFe}_3\(\text{BO}_3\)_4\$ \(R = Y, Ho\): a neutron diffraction and magnetization study](#)
C Ritter, A Vorotynov, A Pankrats *et al.*
- [Determination of the magnetic structure of \$\text{SmFe}_3\(\text{BO}_3\)_4\$ by neutron diffraction: comparison with other \$\text{RFe}_3\(\text{BO}_3\)_4\$ iron borates](#)
C Ritter, A Pankrats, I Gudim *et al.*

Recent citations

- [High-resolution optical spectroscopy and modeling of spectral and magnetic properties of multiferroic \$\text{ErFe}_3\(\text{BO}_3\)_4\$](#)
M. N. Popova *et al*
- [High-resolution spectroscopy of rare-earth ferrobates with a huntite structure](#)
M. N. Popova
- [Optical and magnetic properties of the ground state of \$\text{Cr}^{3+}\$ doping ions in \$\text{REM}_3\(\text{BO}_3\)_4\$ single crystals](#)
A. A. Prokhorov *et al*



IOP | ebooks™

Bringing together innovative digital publishing with leading authors from the global scientific community.

Start exploring the collection—download the first chapter of every title for free.

Phase transitions and crystal-field and exchange interactions in $\text{TbFe}_3(\text{BO}_3)_4$ as seen via optical spectroscopy

M N Popova¹, T N Stanislavchuk², B Z Malkin³ and L N Bezmaternykh⁴

¹ Institute of Spectroscopy, Russian Academy of Sciences, Troitsk, Moscow region, 142190, Russia

² Department of Physics, New Jersey Institute of Technology, Newark, NJ 07102, USA

³ Kazan Federal University, Kazan, 420008, Russia

⁴ Kirenskii Institute of Physics, Siberian Branch of RAS, Krasnoyarsk, 660036, Russia

E-mail: popova@isan.troitsk.ru

Received 21 January 2012, in final form 16 March 2012

Published 17 April 2012

Online at stacks.iop.org/JPhysCM/24/196002

Abstract

High-resolution polarized broadband (1800–23 000 cm^{-1}) optical absorption spectra of Tb^{3+} in $\text{TbFe}_3(\text{BO}_3)_4$ single crystals are studied between room temperature and 4.2 K. The spectral signatures of the structural ($R32$ – $P3_121$, $T_S = 192$ K) and magnetic ($T_N = 41$ K) phase transitions are found and analyzed. Energies and symmetries of the Tb^{3+} crystal-field (CF) levels were determined for both the high-temperature $R32$ and the low-temperature $P3_121$ structures of $\text{TbFe}_3(\text{BO}_3)_4$ and compared with the calculated ones. It follows unambiguously from the spectral data that the ground state is the $\Gamma_1 + \Gamma_2$ quasi-doublet of the local D_3 point symmetry group for Tb^{3+} in the $R32$ high-temperature structure. The CF calculations revealed the CF parameters and wavefunctions for Tb^{3+} in $\text{TbFe}_3(\text{BO}_3)_4$. The value of the Tb–Fe exchange integral and of the effective magnetic field created by the ordered Fe subsystem were estimated as $J_{\text{fd}} = 0.26$ K and $B_{\text{eff}} = 3.92$ T, using the observed splitting $\Delta = 32$ cm^{-1} of the Tb^{3+} ground quasi-doublet at the temperature 5 K. The reliability of the obtained parameters was proven by modeling the literature data on the magnetic susceptibility of $\text{TbFe}_3(\text{BO}_3)_4$. Lattice distortions below T_S were evidenced by the observed changes of probabilities of the forced electric dipole transitions of Tb^{3+} .

(Some figures may appear in colour only in the online journal)

1. Introduction

The family of iron borates with the chemical formula $\text{RFe}_3(\text{BO}_3)_4$ (R—rare earth or yttrium) has attracted considerable attention during the last few years. These materials with rare-earth (RE) ions incorporate two interacting magnetic subsystems, Fe and RE ones, and demonstrate a great variety of interesting magnetic and optical properties and a series of phase transitions occurring with variation of both temperature and external magnetic field [1–13]. Moreover, magnetoelectric coupling and multiferroic features, i.e. the coexistence of at least two of the three order parameters, elastic, magnetic, and electric ones, have been reported for the majority of them [3, 8, 13–17].

RE iron borates crystallize in the trigonal noncentrosymmetric $R32$ (D_3^7) structure of the natural mineral huntite [18] and contain helicoidal chains of edge-sharing FeO_6 octahedra along the trigonal c axis, interconnected by the BO_3 triangles and isolated RO_6 prisms. The R^{3+} ion occupies a single D_3 symmetry position inside the prism and has no direct R–O–R bonds with other R ions through one oxygen atom [18–20]. While for ‘big’ RE ions Pr, Nd, and Sm the $R32$ structure persists down to the lowest temperatures [3, 21, 22], for ‘small’ RE ions from Eu to Er and also Y the structure changes to another trigonal but less symmetric $P3_121$ (D_3^4) one upon decreasing the temperature [3, 20, 21]. This change occurs as a first-order phase transition [3] at the temperature T_S , depending almost linearly on the RE ionic radius and varying

from 58 K for the $\text{EuFe}_3(\text{BO}_3)_4$ single crystal to 350 K for the $\text{ErFe}_3(\text{BO}_3)_4$ one [3, 23]. In the $P3_121$ structure there are two types of nonequivalent iron chains and, though a single structural position for the RE ion survives, its symmetry lowers from D_3 to C_2 [20].

Fe spins in all the $\text{RFe}_3(\text{BO}_3)_4$ compounds order antiferromagnetically at $T_N \sim 30\text{--}40$ K [21] into either an easy-axis ($R = \text{Pr, Tb, Dy}$) or an easy-plane ($R = \text{Nd, Sm, Eu, Gd, Ho, Er, and Y}$) magnetic structure [22–26], depending on a single-ion magnetic anisotropy of the RE^{3+} ion [23]. The RE subsystem becomes magnetically polarized via the f–d exchange interaction but, in its turn, imposes a particular type of magnetic structure on the almost isotropic Fe subsystem [23]. In the case of the Gd and Ho iron borates a competition between (weak) anisotropies of the Fe and RE ions leads to a spin-reorientation phase transition at low temperatures [1, 8]. RE^{3+} ions strongly influence not only magnetic but also magnetoelectric properties; however, the nature of the observed strong differences in the magnetoelectric properties of different RE iron borates is not yet clear [13–17]. To understand the physics of magnetoelectric phenomena in RE iron borates, it is important to know (i) the structural peculiarities of these compounds and (ii) the crystal-field (CF) levels and wavefunctions of the RE^{3+} ions as well as RE–Fe exchange parameters.

As for structural peculiarities, a reduction of the crystal lattice symmetry in the magnetically ordered state has been supposed in [14] to account for the observed magnetoelectric effect in $\text{GdFe}_3(\text{BO}_3)_4$ (both $R32$ and $P3_121$ space symmetry groups belong to the class 32, which does not allow a macroscopic electric polarization vector). However, careful Raman scattering study did not show any additional vibrational modes below T_N , which would manifest a further symmetry reduction as compared to the $P3_121$ structure [3]. In recent hard x-ray scattering experiments very weak structural distinctions from the $P3_121$ space group were found for the Y, Gd, and Tb iron borates [11]. Distortions appear at the temperature T_S of the structural phase transition and grow with decreasing temperature until stabilizing at $T \approx T_N$ [11]. Additional structural distortions triggered by the antiferromagnetic ordering in $\text{TbFe}_3(\text{BO}_3)_4$ have recently been shown based on the observed growth of selected spectral line intensity below $T \approx T_N$ [27]. Thus, the data on structural distortions in $\text{TbFe}_3(\text{BO}_3)_4$ are not yet completely clear and are somewhat contradictory.

The energies and symmetries of the CF levels and, then, wavefunctions of the RE^{3+} ions as well as RE–Fe anisotropic exchange parameters have been found from our earlier high-resolution polarized optical measurements on $\text{NdFe}_3(\text{BO}_3)_4$ [28] and $\text{PrFe}_3(\text{BO}_3)_4$ [29, 30]. Both Nd and Pr iron borates have highly symmetric $R32$ crystal structure at all temperatures and undergo the antiferromagnetic second-order phase transition at about 31 K into, however, completely different magnetic structures: an easy-plane one for $\text{NdFe}_3(\text{BO}_3)_4$ [4, 15, 23] and an easy-axis one for $\text{PrFe}_3(\text{BO}_3)_4$ [12, 16, 23, 30].

In the present paper, we consider $\text{TbFe}_3(\text{BO}_3)_4$, which, similar to $\text{PrFe}_3(\text{BO}_3)_4$, comprises a non-Kramers RE

ion and orders into an easy-axis magnetic structure (at 39–41 K) [5–7, 10, 11, 23, 24], but, unlike $\text{PrFe}_3(\text{BO}_3)_4$, exhibits the $R32\text{--}P3_121$ structural phase transition (at $T_S = 198.5$ K [3]). Recently, $\text{TbFe}_3(\text{BO}_3)_4$ was reported to demonstrate a considerable quadratic magnetoelectric effect at room temperature, exceeding the one observed in the high-temperature multiferroic BiFeO_3 and changing its sign upon rotation of the magnetic field through 90° , which might be interesting for possible practical applications, such as spintronics and magnetic memory devices [17]. In [17], the phenomenon was tentatively explained by a contribution from higher CF levels of Tb^{3+} ; however, a detailed knowledge of the low-energy spectrum of $\text{TbFe}_3(\text{BO}_3)_4$ was absent. Similarly, to explain the observed magnetic properties of this promising material, refined CF parameters of Nd^{3+} ions in the D_3 symmetry position in aluminum and iron borates but not of $\text{TbFe}_3(\text{BO}_3)_4$ (Tb in the C_2 symmetry position) were used [7]. Moreover, it is necessary to revise the theoretical approach of [7] because peculiarities of magnetic properties caused by the specific chain structure of RE iron borates cannot be reproduced in the framework of a single-ion molecular field model (note that different values of the same exchange coupling constant for the iron subsystem were introduced in [7] to describe different phenomena). Also, the supposition employed in [7] about the antiferromagnetic character of the exchange interaction between the nearest-neighbor Tb^{3+} and Fe^{3+} ions contradicts the results of neutron scattering measurements [6].

The goal of the present work was to deliver a detailed energy level scheme for Tb^{3+} in $\text{TbFe}_3(\text{BO}_3)_4$, in both paramagnetic and antiferromagnetic states, using high-resolution optical spectroscopy, and on that basis to perform CF calculations for Tb^{3+} in the C_2 point symmetry site and calculations of the exchange interaction parameters (earlier published absorption spectra of $\text{TbFe}_3(\text{BO}_3)_4$ [5, 27] were of limited spectral range and did not allow to realize this task). The reliability of the obtained parameters was checked by modeling the literature data [6, 17] on the magnetic susceptibility of $\text{TbFe}_3(\text{BO}_3)_4$ in both paramagnetic and antiferromagnetic phases. We also study the temperature dependences of the spectral line intensities and analyze them in view of the possible structural distortions below T_S [11] and T_N [27].

2. Experiment

Single crystals of terbium iron borate were grown on the seeds from the solution melts on the base of $\text{Bi}_2\text{Mo}_3\text{O}_{12}$, as described in [31]. To prepare samples for spectroscopic measurements, we cut out 0.5–1.3 mm thick plates either perpendicular or parallel to the crystallographic c axis of the crystal. Absorption spectra were registered using Fourier-transform spectrometers Bruker 125HR and Bomem DA3.002 in wide spectral ($1800\text{--}23\,000\text{ cm}^{-1}$) and temperature ($4.2\text{--}300$ K) regions with a spectral resolution up to 0.5 cm^{-1} . We used either unpolarized radiation propagating along the crystallographic c axis ($\mathbf{k} \parallel c$, $\mathbf{E}, \mathbf{H} \perp c$, α polarization) or linearly polarized radiation incident perpendicular to the

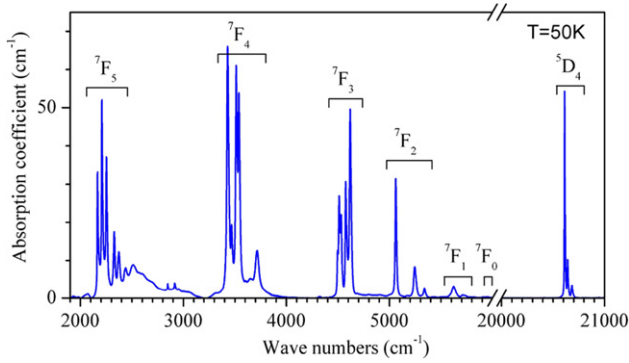


Figure 1. Absorption spectrum of the Tb^{3+} ions in paramagnetic $\text{TbFe}_3(\text{BO}_3)_4$ at $T = 50$ K.

c axis ($\mathbf{k} \perp c$, $\mathbf{E} \perp c$, σ polarization, $\mathbf{k} \perp c$, $\mathbf{E} \parallel c$, π polarization). For cryogenic measurements we used either an optical helium-vapor cryostat or a closed-cycle Cryomech ST-403 cryostat.

3. Results of experiments in paramagnetic phase

Figure 1 shows the absorption spectrum of the Tb^{3+} ions in $\text{TbFe}_3(\text{BO}_3)_4$ in the whole spectral region studied at $T = 50$ K. To obtain this spectrum, we subtracted the absorption spectrum of $\text{GdFe}_3(\text{BO}_3)_4$ (the Gd^{3+} ion does not have energy levels up to $32\,000\text{ cm}^{-1}$ [32]) from the absorption spectrum of $\text{TbFe}_3(\text{BO}_3)_4$. It is worth mentioning that the Tb^{3+} ion has several multiplets in the infrared region. As this is just the region where Fourier-transform spectroscopy implements all its advantages over other spectral methods, the application of Fourier-transform spectroscopy to achieve our goal is the most reasonable [33].

3.1. Spectral signature of the structural phase transition in $\text{TbFe}_3(\text{BO}_3)_4$

At room temperature, the terbium iron borate is in the $R32$ phase. With decreasing temperature, this crystal undergoes the first-order structural phase transition from the $R32$ phase into the $P3_121$ one [3, 20]. In the $R32$ phase, the Tb^{3+} ion occupies the D_3 symmetry position, which is characterized by the threefold axis C_3 directed along the crystal c axis and by three twofold axes C_2 , which are perpendicular to the c axis and form $2\pi/3$ angles with each other as shown in figure 2. In the low-symmetry phase ($P3_121$), the C_3 axis disappears and only one of the three C_2 axes survives; the symmetry of the Tb^{3+} position lowers to the point symmetry group C_2 . As all the twofold axes of the D_3 position are equivalent, there are three equivalent but differently oriented C_2 positions of Tb^{3+} in the primitive cell below T_S [19].

Earlier, the structural phase transition in the $\text{TbFe}_3(\text{BO}_3)_4$ crystal was evidenced by an abrupt appearance of extra phonon lines in the Raman spectra, with a hysteresis loop for the intensities of the new modes versus temperature, centered at T_S [3]. Figure 3 shows that also the spectra of the f–f electronic transitions of the Tb^{3+} ion in $\text{TbFe}_3(\text{BO}_3)_4$

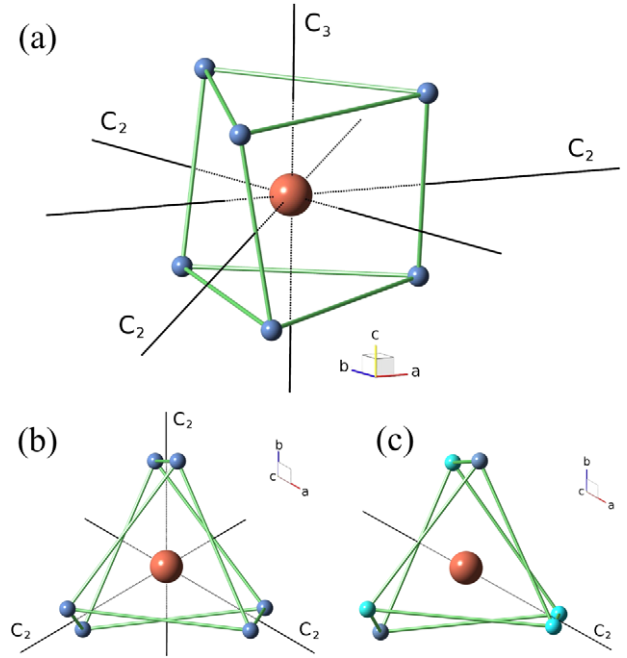


Figure 2. (a) TbO_6 polyhedron in the $R32$ structure and (b) its ab projection at $T > T_S$ (D_3 position). The C_3 axis is parallel to the c axis of the crystal, while the three equivalent C_2 axes lie in the ab plane and form $2\pi/3$ angles with each other. (c) ab projection at $T < T_S$ (C_2 position in the $P3_121$ structure). Only one C_2 axis survives, resulting in three equivalent but differently oriented positions.

above and below T_S differ drastically (compare figures 3(a) and (b)), which points to considerable changes of the crystal field experienced by the Tb^{3+} ion. Figure 4 displays the temperature dependence of the 1E line position in a cooling–heating cycle in the vicinity of T_S . The hysteresis loop is observed, in agreement with Raman scattering data of [3]. The dielectric constant ϵ_c measured at the frequency of 1 kHz [10] is also shown, together with our data on the position of a peak in the interference pattern observed in the α -polarized spectrum of a sample with plane-parallel faces. The wavelength λ_m corresponding to the m th maximum in the interference pattern comes from the equation $2l_c n_o = m\lambda_m$, where l_c is the sample’s thickness and $n_o = \sqrt{\epsilon_{ab}}$ is the refractive index for the ordinary ray propagating along the crystal c axis. The observed pronounced shift of an interference maximum at the structural phase position is connected with a change of the optical path difference $l_c n_o$. The changes of both ϵ_{ab} at optical frequencies and of l_c at T_S may contribute.

3.2. Crystal-field levels of Tb^{3+} in $\text{TbFe}_3(\text{BO}_3)_4$ above T_S (the $R32$ structure)

Before considering the observed spectra, we present below some symmetry information. Wavefunctions of the non-Kramers Tb^{3+} ion above T_S transform according to the Γ_1 and Γ_2 non-degenerate and the Γ_3 doubly degenerate irreducible representations (IRREPs) of the D_3 point symmetry group. Below T_S , the degeneracy of the Γ_3 doublets is lifted

Table 1. Selection rules for the electric dipole (ED) and magnetic dipole (MD) transitions of a non-Kramers ion in the D_3 and C_2 positions. For D_3 , the z axis is parallel to the c axis of the crystal ($z \parallel c$) but the x axis is parallel to the a axis, which coincides with the C_2 axis ($x \parallel a \parallel C_2$). For C_2 , $z' \parallel a$, $x' \parallel b$, $y' \parallel c$.

	ED			MD		
	Γ_1	Γ_2	Γ_3	Γ_1	Γ_2	Γ_3
D_3						
Γ_1	—	d_x π	d_x, d_y α, σ	—	μ_x σ	μ_x, μ_y α, π
Γ_2	d_z π	—	d_x, d_y α, σ	μ_z σ	—	μ_x, μ_y α, π
Γ_3	d_x, d_y α, σ	d_x, d_y α, σ	d_x, d_y, d_z α, σ, π	μ_x, μ_y α, π	μ_x, μ_y α, π	μ_x, μ_y, μ_z α, σ, π
C_2	γ_1	γ_2		γ_1	γ_2	
γ_1	$d_{z'}$ α, σ	$d_{x'}, d_{y'}$ α, σ, π		$\mu_{z'}$ α, π	$\mu_{x'}, \mu_{y'}$ α, σ, π	
γ_2	$d_{x'}, d_{y'}$ α, σ, π	$d_{z'}$ α, σ		$\mu_{x'}, \mu_{y'}$ α, σ, π	$\mu_{z'}$ α, π	

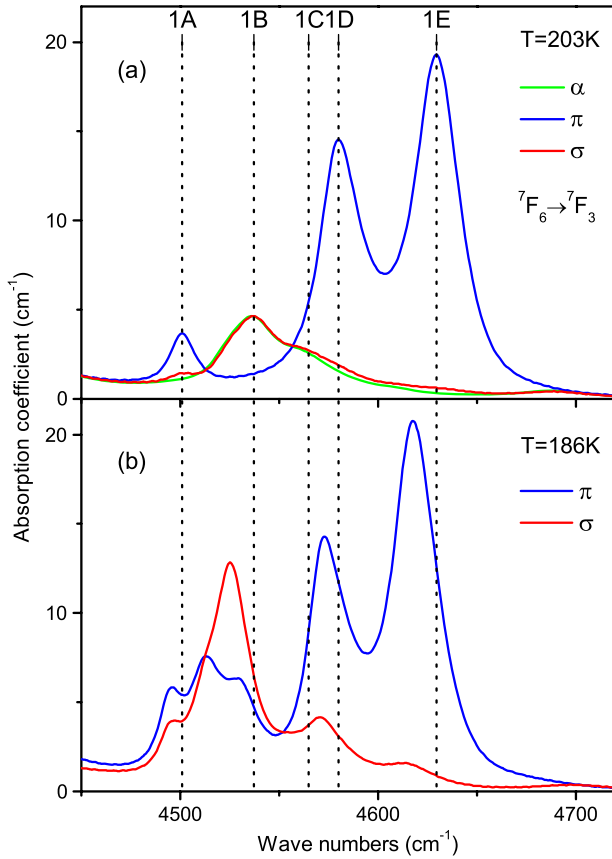


Figure 3. The ${}^7F_6 \rightarrow {}^7F_3$ infrared multiplet of Tb^{3+} in $TbFe_3(BO_3)_4$ for the α -, σ -, and π -polarized radiation, above and below the temperature T_S of the structural phase transition: (a) $T = 203 \text{ K} > T_S$ and (b) $T = 186 \text{ K} < T_S$.

and wavefunctions of all the Tb^{3+} states belong to the non-degenerate γ_1 or γ_2 IRREPs of the C_2 point symmetry group. Selection rules for electric and magnetic dipole (ED and MD) optical transitions between the Tb^{3+} levels in the D_3 and C_2 positions are collected in table 1.

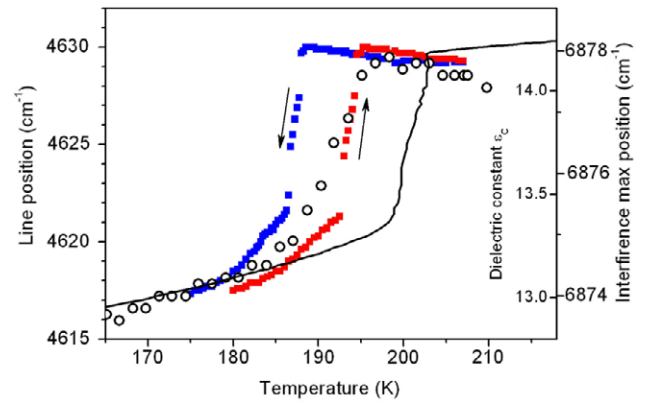


Figure 4. Position of line 1E in the ${}^7F_6 \rightarrow {}^7F_3$ multiplet versus temperature (squares) in a cooling and heating cycle; temperature dependences of the Fabry–Perot interference maximum (open circles) and of the dielectric permeability ϵ_c presented in [10] (solid line).

We consider now the ${}^7F_6 \rightarrow {}^7F_3$ optical multiplet of the Tb^{3+} ion residing in the D_3 symmetry position of the $TbFe_3(BO_3)_4$ crystal at $T = 203 \text{ K} > T_S$ (figure 3(a)). The D_3 symmetry crystal field splits the 7F_3 level of the free Tb^{3+} ion into five sublevels: ${}^7F_3 = \Gamma_1 + 2\Gamma_2 + 2\Gamma_3$. Our temperature-dependent spectra have shown that the ‘hot’ spectral lines originating from the excited CF states of the ground multiplet (2E, 3E, 2D etc in figure 5) do not overlap the spectrum from the ground CF level, which facilitates the line identification. First of all we note that at least two lines (1A and 1E) are silent in the α -polarized spectrum, which rules out the Γ_3 symmetry of the ground state (see table 1). The α -polarized spectrum consists of two lines (1B and 1C) that have the same intensity also in the σ -polarized spectrum. It follows immediately from the selection rules for the D_3 symmetry that these lines correspond to the transitions from either the Γ_1 or the Γ_2 ground state to the two Γ_3 levels and that these are ED transitions. Further, if the ground state were Γ_1 (Γ_2), we would observe two (one) π -polarized lines. The observed three π -polarized lines unambiguously show

Table 2. Measured and calculated CF energies (in cm^{-1}) of the Tb^{3+} ion in $\text{TbFe}_3(\text{BO}_3)_4$, E and $E + \Delta E$ in paramagnetic $R32$ and $P3_121$ phases, respectively, and $E + \Delta E + \Delta E_m$ in the antiferromagnetic phase.

$2S+1L_J$	Experiment			Theory ^{a, b}		
	$T = 203 \text{ K}$	$T = 50 \text{ K}$	$T = 5 \text{ K}$	$T > T_S$	$T_S > T > T_N$	$T_N > T \rightarrow 0$
	E	$E + \Delta E$	ΔE_m	E	$E + \Delta E$	ΔE_m
1	2	3	4	5	6	7
7F_6	0	0	-16	0 ($1\Gamma_1$)	0	-16
	0	0	16	0.181 ($1\Gamma_2$)	0.194	+15.8
	—	196 $T = 100 \text{ K}$	—	208.7 ($1\Gamma_3$)	200 ± 3.3	$+4.4 \pm 1.7$
	—	225 $T = 100 \text{ K}$	—	245.7 ($2\Gamma_1$)	218.2	-0.5
	—	247 $T = 100 \text{ K}$	—	249.8 ($2\Gamma_3$)	245.3 ± 9.6	$+0.4 \mp 0.1$
	—	360 $T = 186 \text{ K}$	—	366.7 ($3\Gamma_3$)	353 ± 1.3	-2.6 ± 3.2
	—	—	—	374.4 ($2\Gamma_2$)	359.5	+1.8
	—	—	—	391.0 ($3\Gamma_1$)	371.3	+2.7
7F_5	—	400 $T = 186 \text{ K}$	—	395.1 ($4\Gamma_3$)	396.8 ± 1.3	$+0.2 \pm 5.9$
	2179 σ	2165.5 ^c	-12.5 ^d	2172.5 ($1\Gamma_3$)	2164.4 ± 0.2	-0.1 ± 9.8
	2220 π	2207.7	-1.7	2216.7 (Γ_1)	2208	-0.9
	2265 π	2252	+3	2271.8 ($1\Gamma_2$)	2258.5	+0.6
	2335 σ	2328 ^c	-10 ^d	2334.3 ($2\Gamma_3$)	2328.5 ± 1	-0.7 ± 5.7
	2392 σ	2372.5 ^c	-15.5 ^d	2385.7 ($3\Gamma_3$)	2378 ± 0.2	$+0.1 \pm 9.9$
	—	—	—	2422.9 ($4\Gamma_3$)	2412.9 ± 5.7	$+0.1 \pm 0.3$
	—	2434	+3	2438.1 ($2\Gamma_2$)	2429	+0
7F_4	3455 π	3427.5	-1.5	3449.8 ($1\Gamma_1$)	3440.2	-1.1
	3471 σ	3470 ± 4.9	$+1 \pm 3.1$	3465.6 ($1\Gamma_3$)	3456.5 ± 3.1	-0.2 ± 1.6
	3526 π	3510.4	+2.6	3532.3 (Γ_2)	3523.4	+0.7
	3560 σ	3568 ± 31	± 1	3576.3 ($2\Gamma_3$)	3568.3 ± 20	-0.3 ± 0.1
	—	—	—	3691.8 ($3\Gamma_3$)	3683.7 ± 12.4	$+0.1 \pm 2$
	3731 π	3713.2	-0.2	3729.8 ($2\Gamma_1$)	3721	-0.1
7F_3	4501 π	4492.7	+0.3	4505.1 ($1\Gamma_2$)	4498.5	-1.1
	4537 σ	4507.5 ^c	-3.5 ^d	4521.4 ($1\Gamma_3$)	4511.8 ± 6.6	-0.5 ± 0.7
	4565 σ	4525.8 ± 2	$+3.4 \pm 1.2$	4541.2 ($2\Gamma_3$)	4533.7 ± 3	$+0.5 \pm 0.5$
	4580 π	4571.2	-0.2	4580.2 ($1\Gamma_1$)	4571.6	-0.6
	4630 π	4614	+4	4633.4 ($2\Gamma_2$)	4623.3	+0.8
	7F_2	5068 π	5056.6	-0.6	5081.1 (Γ_1)	5073.5
5259 σ		5245.4 ± 5	-0.4 ± 1	5260.1 ($1\Gamma_3$)	5250.2 ± 5.1	$+0.2 \pm 0.4$
5352 σ		5334.3 ^c	-3.3 ^d	5351.2 ($2\Gamma_3$)	5343 ± 1.4	$+0 \pm 0.9$
7F_1		5626 π	5617.7	-0.7	5643 (Γ_2)	5638.9
	5738 σ	5720.2 ± 13.5	-0.7 ± 3	5747 (Γ_3)	5737.2 ± 13.3	$+0.1 \pm 0.5$
7F_0	—	5946	+1	5932 (Γ_1)	5922.8	+0.3
5D_4	20616 π	20607.6	-7.3	20597 ($1\Gamma_1$)	20588	-4
	20623 π	20613.8	-11.3	20611 (Γ_2)	20602	+3
	20621 σ	20613.4 ± 4.1	-10 ± 0.2	20629 ($1\Gamma_3$)	20621 ± 5	-3 ± 1
	20650 σ	20639.5 ^c	-12.5 ± 7.5	20641 ($2\Gamma_3$)	20633 ± 5.5	$+3 \pm 1$
	20694 σ	20681.3 ^c	$+1 \pm 4.7$	20698 ($3\Gamma_3$)	20688 ± 1.5	$+2.5 \pm 2.5$
	20712 π	20698.5	-0.5	20720 ($2\Gamma_1$)	20710	0

^a The numbers $a \pm b$ listed for the Γ_3 states in column 6 represent energies $a + b$ and $a - b$ for the two sublevels of the corresponding state in the lower symmetry site.

^b The numbers $a_m \pm b_m$ listed for the Γ_3 states in column 7 give the shift of the center of gravity and additional magnetic splitting of the corresponding sublevels with respect to the values given in column 6, the calculated energies at $T \ll T_N$ equal $a + a_m + b + b_m$ and $a + a_m - b - b_m$.

^c The splitting of the Γ_3 level was not resolved.

^d The lower Γ_3 sublevel.

that the ground state of the Tb^{3+} ion in the high-temperature $R32$ phase is a quasi-doublet $\Gamma_1 + \Gamma_2$, the same as in the case of the $\text{TbAl}_3(\text{BO}_3)_4$ and $\text{YAl}_3(\text{BO}_3)_4:\text{Tb}$ crystals [34, 35]. A small σ component of line 1A comes, evidently, from the MD contribution. Column 2 of table 2 lists the energies of the Tb^{3+} CF levels in the high-temperature $R32$ phase of $\text{TbFe}_3(\text{BO}_3)_4$.

At the $R32$ – $P3_121$ structural phase transition the symmetry of the Tb^{3+} site lowers from D_3 to C_2 , the

degeneracy of the Γ_3 doublets is lifted, and the selection rules are relaxed (see table 1). The 7F_3 multiplet splits into seven singlets: ${}^7F_3 = 3\gamma_1 + 4\gamma_2$. Thus, seven lines should be observed in the spectrum of figure 3(b) at $T = 186 \text{ K} < T_S$. However, only five lines are observed in each polarization and their positions coincide in the π and σ spectra, except the line near 4530 cm^{-1} , where a shift of about 4 cm^{-1} can be detected between the two spectra. Thus, six instead of seven lines can be seen in the spectra of figure 3(b). Probably,

Tb³⁺ ion. In the low-temperature $P3_121$ structure, the CF Hamiltonian contains an additional component of the C_2 symmetry,

$$H_{CF} = H_{CF}(D_3) + \Delta H_{CF}(D_3) + H_{CF}(C_2), \quad (4)$$

which is defined by nine CF parameters B_q^p with $q = -1, 2, 4, -5$:

$$\begin{aligned} H_{CF}(C_2) = & \sum_k [iB_{-1}^2(C_{-1}^{(2)}(k) + C_1^{(2)}(k)) + B_2^2(C_{-2}^{(2)}(k) \\ & + C_2^{(2)}(k)) + iB_{-1}^4(C_{-1}^{(4)}(k) + C_1^{(4)}(k)) + B_2^4(C_{-2}^{(4)}(k) \\ & + C_2^{(4)}(k)) + B_4^4(C_{-4}^{(4)}(k) + C_4^{(4)}(k)) + iB_{-1}^6(C_{-1}^{(6)}(k) \\ & + C_1^{(6)}(k)) + B_2^6(C_{-2}^{(6)}(k) + C_2^{(6)}(k)) + B_4^6(C_{-4}^{(6)}(k) \\ & + C_4^{(6)}(k)) + iB_{-5}^6(C_{-5}^{(6)}(k) + C_5^{(6)}(k))]. \end{aligned} \quad (5)$$

Due to the crystal lattice reconstruction at T_S , parameters of the CF component of the D_3 symmetry in $R32$ and $P3_121$ structures are different. However, according to our estimates based on variations of distances between the Tb³⁺ ion and its nearest-neighbor oxygen ions with temperature from $T = 200$ K ($T > T_S$) to $T = 100$ K ($T < T_S$) measured in neutron scattering experiments [6], relative changes of the CF parameters B_q^p and B_q^6 ($q = 0, -3, 6$) are rather small, and we take into account only one term in $\Delta H_{CF}(D_3)$, namely $\Delta B_0^2 C_0^{(2)}$, that involves substantial contributions from the long-range electrostatic interactions between the Tb³⁺ ion and its distant neighbors.

It was shown in our previous study of CF energies of the Nd³⁺ ion in NdFe₃(BO₃)₄ that calculations in the framework of the exchange charge model brought about reliable values of the five parameters B_q^p ($p = 4, 6$) in the CF Hamiltonian (3) for the $R32$ structure [28]. In the present work, we also calculated 12 CF parameters B_q^p ($p = 4, 6$) of the Hamiltonian (4) in the framework of the exchange charge model using the structural data for TbFe₃(BO₃)₄ from [6]. As for the three parameters B_q^2 of the quadrupole CF component which depend critically on the electron density distribution in the crystal lattice, the B_0^2 parameter is determined unambiguously by the gap (~ 100 cm⁻¹) between the Γ_3 and Γ_2 sublevels of the ⁷F₁ multiplet at $T > T_S$; the ΔB_0^2 , B_{-1}^2 and B_2^2 parameters are obtained from fitting the splittings of the ⁷F₁ multiplet and $1\Gamma_3$ (⁷F₂) doublet keeping fixed values of the calculated parameters B_q^4 and B_q^6 . The following set of the CF parameters (in cm⁻¹) was obtained:

$$\begin{aligned} B_0^2 &= 464, & \Delta B_0^2 &= -30 & B_0^4 &= -1256, \\ B_0^6 &= 352, & B_{-3}^4 &= 608.5, & B_{-3}^6 &= 73, \\ & & B_6^6 &= 270, & & \end{aligned} \quad (6a)$$

$$\begin{aligned} B_{-1}^2 &= 38.4 & B_{-1}^4 &= -66, & B_{-1}^6 &= -27, \\ B_2^2 &= 54, & B_2^4 &= 82, & B_2^6 &= -8, \\ B_4^4 &= -23, & B_4^6 &= -27, & B_{-5}^6 &= -91. \end{aligned} \quad (6b)$$

As follows from a comparison of the parameters (6a) with the corresponding parameters for Pr³⁺ in PrFe₃(BO₃)₄ [30] and for Nd³⁺ in NdFe₃(BO₃)₄ [28], the CF parameters in the

$R32$ structure vary monotonically with change of the atomic number and, hence, the ionic radius of the RE ion.

Eigenvalues and eigenfunctions of the Hamiltonian (1) were found by a numerical diagonalization of the Hamiltonian matrix in a complete basis of 3003 states of the 4f⁸ electronic configuration. The calculated CF energies for the ⁷F_J and ⁵D₄ multiplets of Tb³⁺ in the $R32$ and $P3_121$ structures are listed in table 2 (columns 5 and 6, respectively). Splittings of the Γ_3 doublets caused by the crystal field of the C_2 symmetry are presented explicitly in column 6. Data in column 6 are to be compared to the measured energies in column 3. It is seen that agreement is satisfactory apart from relative shifts up to 20 cm⁻¹ between centers of gravity of several upper multiplets (⁷F₂, ⁷F₁, ⁷F₀, ⁵D₄). Reliability of the results is confirmed by the agreement of the levels' symmetry properties that follow from the CF calculations and from the measured polarized spectra.

According to the results of calculations, the gap $\delta = 0.28$ K between the two lowest singlets is rather small, excited CF sublevels lie at about 280 K higher in energy relative to the ground quasi-doublet, and magnetic properties of the Tb³⁺ ion in the local system of coordinates defined above are well described at low temperatures by the effective spin Hamiltonian ($S = 1/2$)

$$H_S = \delta S_x + \mu_B (g_{yz} B_y + g_{zz} B_z) S_z \quad (7)$$

where μ_B is the Bohr magneton, \mathbf{B} is the external magnetic field, and g_{yz} and g_{zz} are non-zero components of the highly anisotropic magnetic g factor. The values $g_{yz} = 0.62 \pm 0.01$ and $g_{zz} = 17.5 \pm 0.3$ have been obtained from matrix elements of the Tb³⁺ magnetic moment $\mathbf{m} = -\mu_B \sum_k (\xi \mathbf{l}_k + 2\mathbf{s}_k)$ (here \mathbf{l}_k and \mathbf{s}_k are orbital and spin moments, respectively, of the k th 4f electron, and $\xi = 0.96 \pm 0.04$ is the orbital reduction factor) computed in the basis of eigenfunctions of the Hamiltonian (1). The value of the orbital reduction factor was estimated from a comparison of the calculated magnetic moment of the Tb³⁺ ion with the measured saturated moment of $8.6 \mu_B$ given in [6].

5. Spectral and magnetic properties of TbFe₃(BO₃)₄ in the antiferromagnetic phase

5.1. Spectroscopic detection of magnetic ordering

On lowering the temperature below ~ 40 K, some spectral lines split into two components as shown in figure 6 for the example of the ⁷F₆ → ⁷F₂ transition. Decrease of the intensity of the low-frequency components of the split lines and the fact that the splitting value is the same for all spectral lines that terminate at the singlets of the $R32$ phase confirm our conclusion (see section 3.1) about the quasi-doublet (i.e. two closely separated levels) in the ground state. The population of the upper sublevel of the split quasi-doublet decreases with decreasing temperature, leading to a decrease of the intensity of the low-frequency components of the split spectral lines and to a Schottky-type anomaly in the temperature dependence of the specific heat of TbFe₃(BO₃)₄ measured in [7].

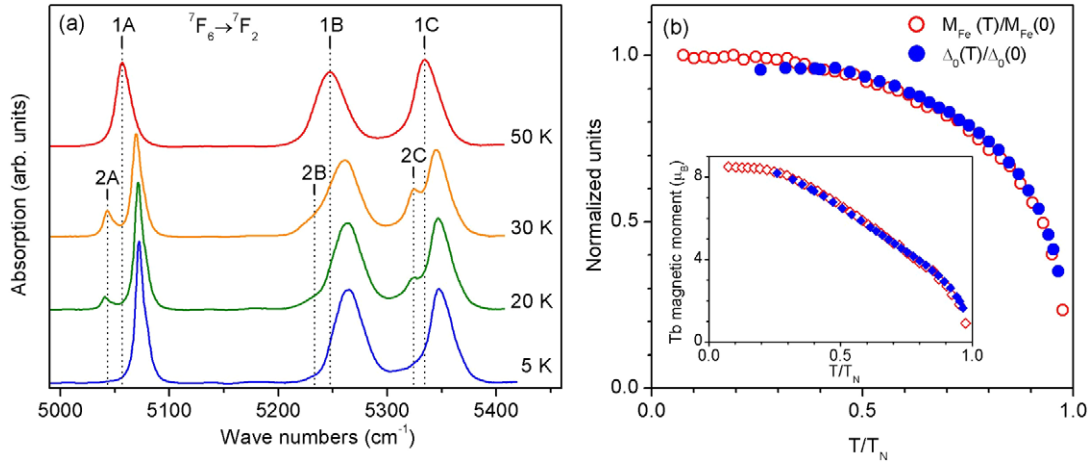


Figure 6. (a) The splitting of spectral lines of the ${}^7F_6 \rightarrow {}^7F_2$ infrared transition of Tb^{3+} and (b) the temperature dependences of the ground-state splitting, $\Delta(T)/\Delta(0)$, $\Delta(0) = 32 \text{ cm}^{-1}$, obtained from the spectral data (solid circles), and of iron magnetic moment, measured in neutron scattering experiments [6], $M_{Fe}(T)/M_{Fe}(0)$, $M_{Fe}(0) = 4.4 \mu_B$ (open circles). The inset of (b) presents the terbium magnetic moment calculated (see the text) from the observed splitting $\Delta(T)$ (solid circles) and measured in neutron experiments [6] (open circles).

The observed splitting of the quasi-doublet is due to magnetic ordering of the iron subsystem at $T_N \sim 40 \text{ K}$ [24]. The Hamiltonian of the f-d exchange interaction between the Tb^{3+} ion and the nearest-neighbor Fe^{3+} ion (which is the S-state ion with zero orbital moment in the ground state) has the following form [40]:

$$H_{Tb-Fe} = \sum_k A(\mathbf{l}_k) \mathbf{s}_k \cdot \mathbf{S}_{Fe}. \quad (8)$$

Here \mathbf{S}_{Fe} ($S = 5/2$) is the spin moment of the Fe^{3+} ion. In the present work, we consider only isotropic exchange interactions between the Tb^{3+} ion and its six nearest-neighbor Fe^{3+} ions approximating the operator $A(\mathbf{l}_k)$ by a constant, $A(\mathbf{l}_k) = -2J_{fd}$. So, we neglect the dependence of the exchange energy on the orbital state of the Tb^{3+} ion. As has already been mentioned in section 1, there are two types of nonequivalent helicoidal chains of the FeO_6 octahedra in the crystal lattice with the $P3_121$ space symmetry group containing the Fe^{3+} ions at sites with the C_2 (Fe1) and C_1 (Fe2) local symmetries, respectively. Distances between the Fe1 ions and between the Fe2 ions within the chains are slightly different (0.3177 and 0.3185 nm at $T = 2 \text{ K}$ [6], respectively), and the distances between the Tb^{3+} ion and its nearest-neighbor Fe1 ions (0.376 nm, two ions) and Fe2 ions (0.382 for one pair and 0.370 nm for another pair of Fe2 ions) are different as well [6]. However, to reduce the number of unknown parameters, we neglect differences between the Tb-Fe1 and Tb-Fe2 exchange interactions and assume that all Fe^{3+} ions are in the same crystallographic positions.

According to the neutron scattering data [6], at temperatures $T < T_N$ magnetic moments of the Fe^{3+} ions $\mathbf{M}_{Fe} = -g\mu_B \langle \mathbf{S}_{Fe} \rangle$ ($g = 2$) possess the same direction (parallel to the crystallographic c axis) within the a - b planes, while the Tb magnetic moments belonging to the same plane are antiferromagnetically aligned to them. Within the nearest-neighbor a - b planes, magnetic moments have the opposite directions. This means that the magnetic moment of a Tb^{3+} ion is ferromagnetically coupled to

magnetic moments of the nearest-neighbor Fe^{3+} ions lying in the nearest-neighbor a - b planes, and, correspondingly, the exchange integral J_{fd} has the positive sign. In the framework of the mean-field approximation, we can substitute the average value of the spin moment $\langle \mathbf{S}_{Fe} \rangle$ for the dynamic variable \mathbf{S}_{Fe} in the Hamiltonian (8). Summing the expression (8) over the six Fe^{3+} nearest neighbors of the Tb^{3+} ion, we obtain the effective exchange Hamiltonian $H_{exch} = -\mathbf{F} \cdot \mathbf{M}_{Fe}$, where the operator \mathbf{F} is defined as follows:

$$\mathbf{F} = -\frac{6J_{fd}}{\mu_B} \sum_k \mathbf{s}_k = -\frac{6J_{fd}}{\mu_B} \mathbf{S}_{Tb}. \quad (9)$$

The absolute value of the exchange integral, $J_{fd} = 0.26 \text{ K}$, was determined from a comparison of the splitting of the ground quasi-doublet calculated and measured at $T = 5 \text{ K}$. Figure 6(b) shows the temperature dependence of the quasi-doublet splitting, obtained from the analysis of the spectra, and the spontaneous iron magnetic moment, taken from [6]. Good coincidence of these dependences points to reliability of the approximation used for the exchange interaction.

The energies of the CF levels of the Tb^{3+} ions at low temperatures $T \ll T_N$ obtained using numerical diagonalization of the matrix of the Hamiltonian $H = H_{FI} + H_{CF} - F_z M_{Fe,z}$ are listed in table 2 (see column 7, where we present shifts of the energy levels relative to their positions in the paramagnetic phase with $M_{Fe,z} = 0$). The results of calculations agree qualitatively with the experimental data (table 2, column 4), in particular, the calculated large splittings of the $1\Gamma_3$, $2\Gamma_3$ and $3\Gamma_3$ doublets in the 7F_5 multiplet correlate with the observed large shifts of the corresponding spectral lines. However, there are considerable differences between the calculated and measured energies of the four lower sublevels of the 5D_4 multiplet, but more detailed studies are necessary to identify optical transitions to this multiplet from the ground quasi-doublet (see section 3.2 above).

The ordered iron magnetic moments mainly affect the ground quasi-doublet of the Tb^{3+} ion. Within the

space of states of the ground multiplet 7F_6 , the Tb spin moment operator is proportional to the total angular momentum ($S_{Tb} = (g_J - 1)J_{Tb}$, $g_J = 3/2$ is the Landé factor) and, correspondingly, to the Tb magnetic moment $m = -\mu_B g_J J_{Tb}$. Thus, we can write the exchange Hamiltonian as the Zeeman energy of the Tb^{3+} ion in the effective magnetic field

$$\mathbf{B}_{\text{exch}}(T) = -\frac{12(g_J - 1)J_{\text{fd}}}{g_J\mu_B} \langle S_{\text{Fe}} \rangle. \quad (10)$$

Substituting the value $J_{\text{fd}} = 0.26$ K into (10), we obtain for $T \rightarrow 0$ ($\langle S_{\text{Fe},x} \rangle = \langle S_{\text{Fe},y} \rangle = 0$, $\langle S_{\text{Fe},z} \rangle = \pm 5/2$) the absolute value of the effective field $|B_{\text{exch},z}| = 3.92$ T, which is close to the value of the external magnetic field applied along the c axis that drives the spin-flop transition [6, 7]. Differences between the energies of the Tb^{3+} ion in this exchange field and the energies presented in table 2 (column 7) do not exceed 0.5 cm^{-1} . In particular, the corresponding calculated splitting of the ground quasi-doublet (see (7)) is equal to $\Delta(T \rightarrow 0) = [\delta^2 + (\mu_B g_{zz} B_{\text{exch},z})^2]^{1/2} = 31.8 \text{ cm}^{-1}$. A good coincidence of the temperature dependence of the Tb magnetic moment calculated from the measured ground-state splitting, $m_{Tb}(T) = \mu_{Tb}(0) \tanh \Delta(T)/2kT$, with that measured in the neutron scattering experiments [6] (see inset of figure 6(b)) further supports the model used.

5.2. Spectroscopic search for structural distortions in $TbFe_3(BO_3)_4$

In the free rare-earth ions, MD f–f optical transitions are parity allowed (and should obey the following selection rules in the LS coupling approximation: $\Delta L = 0$, $\Delta S = 0$, $\Delta J = \pm 1$), while the ED ones are strictly forbidden by parity selection rules. For the RE ion in a crystal, odd components of a noncentrosymmetric crystal field admix electronic wavefunctions of the opposite parity (in particular, the 5d and 5g functions) to the 4f wavefunctions, thus relaxing the parity selection rule—‘forced’ ED transitions are allowed. The intensities of the so called ‘hypersensitive transitions’ are the most sensitive to subtle changes in the nearest environment of the RE ion [41]. In search of such temperature-dependent changes of spectral line intensities, we have measured the integrated intensity of the hypersensitive 7F_6 – 5D_4 optical transition of Tb^{3+} in $TbFe_3(BO_3)_4$. More precisely, the intensities of all the transitions from the ground quasi-doublet to the CF levels of the 5D_4 multiplet were measured (the ‘hot’ lines do not overlap the main lines of this relatively narrow multiplet). Figure 7 shows these intensities divided by the temperature-dependent population of the ground quasi-doublet (normalized integral intensities proportional to the transition probability). Within the precision of our measurements, the result is temperature independent. Thus, the integral intensity of the Tb^{3+} optical 5D_4 multiplet is insensitive to slight crystal lattice deformation and, in particular, deviations of the Fe^{3+} ions, Fe2, from the C_2 symmetry positions below T_S [6, 11]. Neither does it point to any distortions in the magnetically ordered phase. The intensity changes of the two lowest-frequency lines of the 5D_4 optical multiplet observed in [27] below T_N were,

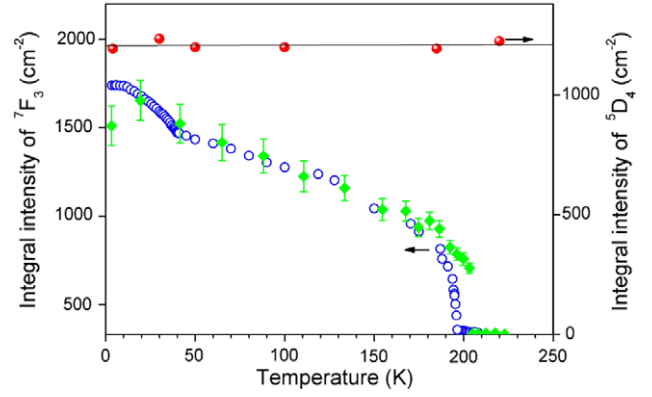


Figure 7. Integral intensity of all the transitions from the ground quasi-doublet to the 5D_4 (solid circles) and 7F_3 (open circles) levels, divided by the relative population of the ground quasi-doublet. Diamonds show the normalized intensity of the (0, 0, 1) reflection in the hard x-ray experiments [11] manifesting deviations from the $P3_121$ structure.

probably, caused by the intensity borrowing from neighboring transitions due to mixing of wavefunctions of different CF levels by the effective magnetic field \mathbf{B}_{exch} created by the ordered Fe spins [29].

The 7F_6 – 7F_3 infrared multiplet is one more ‘narrow’ optical multiplet with main lines not overlapped by the ‘hot’ ones. Again, we have measured the normalized integrated intensity versus temperature for this multiplet (see figure 7). This dependence exhibits pronounced peculiarities at the temperatures of the structural (T_S) and magnetic (T_N) phase transitions. A sudden jump at T_S and a subsequent behavior in the temperature range $T_N < T < T_S$ coincide well with the hard x-ray data [11]. The (001) and (002) x-ray reflections evidenced weak but growing structural distortions from the $P3_121$ structure below T_S [11]. A further growth of the normalized integrated intensity of the 7F_3 multiplet below T_N could be assigned to some additional distortions caused by the magnetic ordering (e.g. via magnetostriction), in the case of equal probabilities of optical transitions from both components of the split ground quasi-doublet. This point needs a special investigation.

5.3. Magnetic susceptibility

Temperature dependences of the static longitudinal and transversal magnetic susceptibilities χ_{\parallel} and χ_{\perp} of $TbFe_3(BO_3)_4$ single crystals for external magnetic fields parallel and perpendicular to the c axis, respectively, have been measured in several laboratories [6, 7, 17]. Because of the very strong magnetic anisotropy of the terbium subsystem, the transversal susceptibility at low temperatures was considerably overestimated in [7], due to a small misalignment of the sample. The results of measurements were used in [7] to estimate the f–d exchange coupling constant and the value $\lambda_{\text{fd}} = -0.253 \text{ T}/\mu_B$ was obtained. The negative sign of λ_{fd} contradicts the magnetic structure of $TbFe_3(BO_3)_4$ determined from the neutron scattering measurements [6]. We obtain a positive λ_{fd} constant with the same absolute

value, according to the relation $\lambda_{fd} = 2(1 - 1/g_J)J_{fd}/\mu_B^2$ and using the quantity $J_{fd} = 0.26$ K obtained in section 5.1 of this paper. In [7], a satisfactory qualitative agreement between the calculated and measured temperature dependences of χ_{\parallel} and χ_{\perp} was achieved in the framework of the single-ion molecular field model neglecting the interaction between iron and terbium subsystems in the paramagnetic phase. However, as has been shown in [28, 30], the f–d exchange brings about an essential renormalization of the susceptibility of the iron subsystem. Just from the explicit consideration of this renormalization and from the comparison of the calculated and measured susceptibilities of $\text{PrFe}_3(\text{BO}_3)_4$, we have predicted earlier [30] the antiferromagnetic f–d coupling between the Pr^{3+} ion and the nearest-neighbor Fe^{3+} ions which was later confirmed by neutron scattering data in [42]. Different values of the molecular field constant corresponding to the exchange interaction between the iron ions ($\lambda_1 = -3$ T/ μ_B , $\lambda_2 = -2$ T/ μ_B) were found in [7] from the analysis of the magnetization dependences on external magnetic field (at $T = 4.2$ K) and temperature; these values were assigned to the intra-chain and inter-chain interactions, respectively. However, in the framework of the single-ion model, contributions to the molecular field constant from inter- and intra-chain interactions are additive and cannot be separated, so no definite conclusions about the relative strengths of these interactions can be obtained. Nevertheless, it is possible to determine parameters of these interactions from a more detailed analysis of the measured temperature dependences of the susceptibilities, as is described below.

We calculated linear responses of the terbium and iron magnetic subsystems coupled by the f–d exchange in the weak external magnetic field \mathbf{B} using the cluster approach derived in our previous studies of $\text{NdFe}_3(\text{BO}_3)_4$ [28] and $\text{PrFe}_3(\text{BO}_3)_4$ [30]. The analytical expression for the effective isotropic susceptibility of the iron ions, χ_d^{Fe} (see (8) in [28]), obtained in the framework of the dimer model, allows us to study separately impacts of the intra-chain (within a Fe–Fe dimer) and inter-chain Fe–Fe exchange integrals, J_{nm} and J_{nmn} , respectively, on the susceptibility. Thus we can consider these integrals as adjustable parameters.

The Tb^{3+} and Fe^{3+} ions belonging to different sublattices in the $P3_121$ structure (there are three terbium and nine iron sublattices) are magnetically nonequivalent in the arbitrarily directed external magnetic field \mathbf{B} . In the paramagnetic phase, the corresponding magnetic moments satisfy the system of self-consistent equations

$$\mathbf{M}_{\text{Tb}(s)} = \chi_{\text{Tb}(s)} \left(\mathbf{B} + \frac{\lambda_{fd}}{2} \sum_{s'} \mathbf{M}_{\text{Fe}(s')} \right), \quad (11)$$

$s = 1-3;$

$$\mathbf{M}_{\text{Fe}(s)} = \chi_d^{\text{Fe}} \left(\mathbf{B} + \frac{\lambda_{fd}}{2} \sum_{s'} \mathbf{M}_{\text{Tb}(s')} \right), \quad (12)$$

$s = 1-9.$

The sums in (11) and (12) are taken over the nearest-neighbor ions (six iron ions and two terbium ions, respectively) belonging to different sublattices. We neglect

here the demagnetizing field and magnetic dipole–dipole interactions because the corresponding contributions to the molecular field constants of the order of $r^{-3} \approx 0.01$ T/ μ_B (r is the distance between the nearest-neighbor magnetic ions) are much less than λ_{fd} . By making use of solutions of (11), (12) and summing magnetic moments of the magnetically nonequivalent ions in the unit cell, we obtain the following expressions for components of the bulk susceptibility tensor (per mole of $\text{TbFe}_3(\text{BO}_3)_4$) valid at the temperatures $T_S > T > T_N$:

$$\chi_{\parallel} = N_A \chi_{\text{Tb},zz} + 3N_A \chi_d^{\text{Fe}} \left[\frac{(1+K)^2}{1-3\hat{\chi}_d^{\text{Fe}}K} + \frac{\hat{\chi}_{\text{Tb},yz}^2}{8-3A_{yy}} \right], \quad (13)$$

$$\chi_{\perp} = \frac{N_A}{2} (\chi_{\text{Tb},xx} + \chi_{\text{Tb},yy}) + N_A \chi_d^{\text{Fe}} \times \left\{ \frac{3}{2(\hat{\chi}_d^{\text{Fe}})^2} D_1 [\beta - 12(4-3A_{xx})DD_1] + \frac{3\hat{\chi}_{\text{Tb},yz}^2}{2(4-3A_{zz})} + D \left[(1 + \hat{\chi}_{\text{Tb},xx})^2 (1 + 9D_1) + 2 \left(1 + \hat{\chi}_{\text{Tb},xx} - 3 \frac{D_1}{\hat{\chi}_d^{\text{Fe}}} D_1 (4-3A_{xx}) \right)^2 \right] \right\}. \quad (14)$$

Here N_A is the Avogadro number, $\hat{\chi}_d^{\text{Fe}} = \lambda_{fd}\chi_d^{\text{Fe}}$, $\hat{\chi}_{\text{Tb},\alpha\beta} = \lambda_{fd}\chi_{\text{Tb},\alpha\beta}$, $A_{\alpha\beta} = \hat{\chi}_d^{\text{Fe}}\hat{\chi}_{\text{Tb},\alpha\beta}$, $K = \hat{\chi}_{\text{Tb},zz} + 3A_{yz}\hat{\chi}_{\text{Tb},yz}(8-3A_{yy})^{-1}$, $\beta = [A_{xx} - A_{yy} - 3A_{yz}^2(4-3A_{zz})^{-1}]$, $D_1 = \beta[4(4-3A_{xx}) + 3\beta]^{-1}$, and $D = [1 - 3A_{xx} + 27(1 - A_{xx})D_1]^{-1}$. It is clearly seen that the renormalized susceptibility of the iron subsystem can be enhanced or suppressed depending on the sign of the f–d exchange coupling constant. For the $R32$ structure (at temperatures $T > T_S$), (13), (14) transform into a simpler formula given by (14) of [30], due to axial symmetry of the tensor χ_{Tb} . In the antiferromagnetic phase (at temperatures $T < T_N$), the longitudinal and transversal components of the susceptibility tensor were simulated with taking into account the spontaneous magnetic moments of the Fe^{3+} ions measured in [6] and the internal magnetic fields (10) affecting the Tb^{3+} ions. The corresponding expressions are similar to (13), (14) but involve, instead of χ_d^{Fe} , the longitudinal and transversal components of the susceptibility tensor of the iron ions (see (20) in [30]).

Non-zero components xx , yy , zz , and yz of the susceptibility tensor χ_{Tb} of the Tb^{3+} ion (in the coordinate frame with $x \parallel C_2$ and $z \parallel c$) in the crystal fields given by (3) (for $T > T_S$) and (4) (for $T < T_S$) and in the internal magnetic field ($T < T_N$) were computed with the step of 1 K. The calculated susceptibilities are presented in figure 8.

As seen in figure 8, the measured temperature dependences of the susceptibilities χ_{\parallel} and χ_{\perp} of $\text{TbFe}_3(\text{BO}_3)_4$ single crystals in the antiferromagnetic $P3_121$, paramagnetic $P3_121$ and $R32$ phases are satisfactorily reproduced by the results of calculations. We used the temperature-independent Fe–Fe exchange integrals $J_{nm} = -6.7$ K and $J_{nmn} = -2$ K, comparable to the obtained earlier values of these parameters $J_{nm} = -6.25$ K and $J_{nmn} = -1.92$ K in Pr and Nd iron

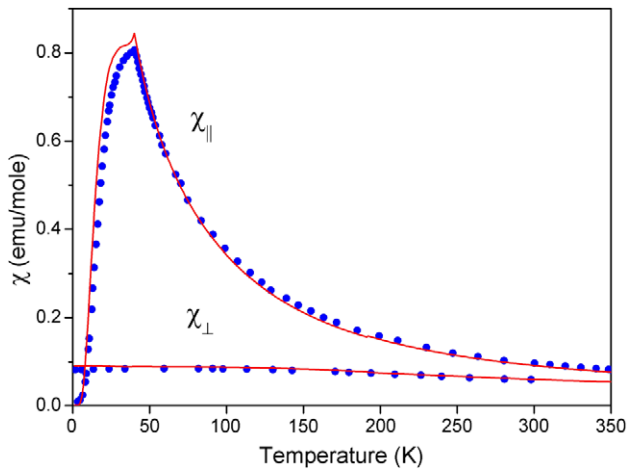


Figure 8. Calculated (solid curves) temperature dependences of the magnetic susceptibility of $\text{TbFe}_3(\text{BO}_3)_4$ as compared to experimental data (symbols) digitized from [6] and [17].

borates [28, 30]. The value of the molecular field constant for the iron subsystem should be $\lambda = (J_{nn} + J_{nnn})/(3\mu_B^2) = -4.3 \text{ T}/\mu_B$. This value corresponds to the effective exchange field of 64.5 T affecting the iron ions at liquid helium temperatures, in good agreement with the estimate 68 T of this field from the antiferromagnetic resonance measurements in [43], and notably exceeds values of λ_1 and λ_2 obtained in [7].

The noticeable differences between the calculated and measured susceptibilities $\chi_{||}$ at temperatures just below T_N are most likely caused by neglect of differences between magnetic and spectral properties of Fe1 and Fe2 ions in the derived theory. The calculated discontinuities of the susceptibilities at the structural phase transition $[\chi_{||}(T_S + \varepsilon) - \chi_{||}(T_S - \varepsilon)]_{\varepsilon \rightarrow +0} = 3 \times 10^{-3}$ and $[\chi_{\perp}(T_S + \varepsilon) - \chi_{\perp}(T_S - \varepsilon)]_{\varepsilon \rightarrow +0} = -1.5 \times 10^{-3} \text{ emu mol}^{-1}$ have the correct signs, but their absolute values are about twice the results of measurements in [6]. The discontinuities of the susceptibilities are caused mainly by shifts of the CF energies due to the change of the parameter B_0^2 at T_S , but one may also expect essential contributions to these discontinuities due to changes of the exchange integrals at T_S which are more sensitive to lengths and directions of the inter-ion bonds than the CF parameters.

6. Conclusion

From the high-resolution polarized temperature-dependent absorption spectra of the terbium iron borate we have determined energies and symmetries of the Tb^{3+} crystal-field levels in both the $R32$ high-temperature phase of $\text{TbFe}_3(\text{BO}_3)_4$ and the $P3_121$ low-temperature one, in the latter case, both above and below the temperature T_N of the magnetic ordering. The CF levels shift markedly at the temperature $T_S = 192 \text{ K}$ of the structural $R32$ – $P3_121$ phase transition, thus evidencing a change of the crystal field and demonstrating a hysteresis loop typical for a first-order phase transition. The structural phase transition is accompanied by an abrupt change of the crystal optical length along the c axis, l_{c0} .

Crystal-field calculations have resulted in CF parameters for Tb^{3+} in the D_3 symmetry position (the $R32$ structure). Though the local symmetry for the Tb^{3+} ion lowers to C_2 in the $P3_121$ low-temperature phase, the spectrum is approximately described by the same set of the CF parameters for the D_3 point symmetry group, with B_0^2 corrected by -6% , to account for the crystal lattice deformation. A more precise modeling of the spectrum, including a description of the observed splittings of the D_3 symmetry doublets into the C_2 symmetry singlets, was achieved by taking into account the whole set of 15 CF parameters for the C_2 point symmetry group. These data can be used to interpret successively magnetic and magnetoelectric properties of this important material. In particular, the measured magnetic susceptibility [6, 17] was modeled in this work. The calculated g -factor for the ground quasi-doublet of the Tb^{3+} ion is highly anisotropic; at low temperatures the magnetic moment is only slightly tilted from the c axis (by the angle $\arctg(g_{yz}/g_{zz}) \sim 2^\circ$), that explains the easy-axis arrangement of both Tb and Fe magnetic moments below T_N .

The magnetic ordering manifests itself by the splitting $\Delta(T)$ of the Tb^{3+} ground-state quasi-doublet, $\Delta(T \rightarrow 0) = 32 \text{ cm}^{-1}$. This splitting is proportional to the magnetic moment of the iron sublattice, which points to applicability of the mean-field model for the terbium sublattice. The Tb^{3+} ions are polarized by the internal magnetic field created by ordered Fe spins. The low-temperature ($T \rightarrow 0$) value of this field was estimated as $|B_{\text{exch},z}| = 3.92 \text{ T}$, which is close to the value of the external magnetic field applied along the c axis that drives the spin-flop transition [6, 7].

The measured integral intensity of the hypersensitive 7F_6 – 5D_4 optical transition of Tb^{3+} did not give any indication of possible structural distortions at low temperatures. In contrast, the growth of the integral intensity of the 7F_6 – 7F_3 infrared transition on lowering the temperature clearly points to lattice distortions below T_S . Optical data follow the same temperature dependence as the intensity of the (0, 0, 1) superlattice reflection in the hard x-ray experiments on $\text{TbFe}_3(\text{BO}_3)_4$ [11]. These x-ray experiments have evidenced deviations from the $P3_121$ lattice symmetry below T_S . In any case, deviations from the $P3_121$ symmetry are small; the Tb^{3+} optical spectra are satisfactorily described in terms of the C_2 local symmetry group.

Acknowledgments

The assistance of E P Chukalina is acknowledged. This work was supported in part by the Russian Foundation for Basic Research (grants No 10-02-01071-a and No 09-02-00171-a), by the Ministry of Education and Science (grant HIII-4828.2012.2), and by the Russian Academy of Sciences under the Programs for Basic Research.

References

- [1] Levitin R Z, Popova E A, Chtsherbov R M, Vasiliev A N, Popova M N, Chukalina E P, Klimin S A, van Loosdrecht P H M, Fausti D and Bezmaternykh L N 2004 *JETP Lett.* **79** 423

- [2] Kalashnikova A M, Pavlov V V, Pisarev R V, Bezmaternykh L N, Bayer M and Rasing Th 2004 *JETP Lett.* **80** 293
- [3] Fausti D, Nugroho A, Loosdrecht P H M, Klimin S A, Popova M N and Bezmaternykh L N 2006 *Phys. Rev. B* **74** 024403
- [4] Fisher P, Pomjakushin V, Sheptyakov D, Keller L, Janoschek M, Roessli B, Schefer J, Petrakovskii G, Bezmaternikh L, Temerov V and Velikanov D 2006 *J. Phys.: Condens. Matter* **18** 7975
Janoschek M, Fisher P, Schefer J, Roessli B, Pomjakushin V, Meven M, Petricek V, Petrakovskii G and Bezmaternikh L 2010 *Phys. Rev. B* **81** 094429
- [5] Popova M N, Chukalina E P, Stanislavchuk T N and Bezmaternykh L N 2006 *Izvestiya RAN. Seriya Fizicheskaya* **70** 1652 (in Russian)
- [6] Ritter C, Balaev A, Vorotynov A, Petrakovskii G, Velikanov D, Temerov V and Gudim I 2007 *J. Phys.: Condens. Matter* **19** 196227
- [7] Popova E A, Volkov D V, Vasiliev A N, Demidov A A, Kolmakova N P, Gudim I A and Bezmaternykh L N 2007 *Phys. Rev. B* **75** 224413
Volkov D V, Popova E A, Kolmakova N P, Demidov A A, Tristan N, Skourski Yu, Buechner B, Gudim I A and Bezmaternykh L N 2007 *J. Magn. Magn. Mater.* **316** e717
- [8] Ritter C, Vorotynov A, Pankrats A, Petrakovskii G, Temerov V, Gudim I and Szymczak R 2008 *J. Phys.: Condens. Matter* **20** 3652009
- [9] Chaundhury R P, Yen F, Lorenz B, Sun Y Y, Bezmaternykh L N, Temerov V L and Chu C W 2009 *Phys. Rev. B* **80** 104424
- [10] Adem U, Wang L, Fausti D, Schottenhamel W, van Loosdrecht P H M, Vasiliev A, Bezmaternykh L N, Buchner B, Hess C and Klingeler R 2010 *Phys. Rev. B* **82** 064406
- [11] Hamann-Borrero J E, Philipp M, Kataeva O V, Zimmermann M, Geck J, Klingeler R, Vasiliev A, Bezmaternykh L, Buchner B and Hess C 2010 *Phys. Rev. B* **82** 094411
- [12] Ritter C, Vorotynov A, Pankrats A, Petrakovskii G, Temerov V, Gudim I and Szymczak R 2010 *J. Phys.: Condens. Matter* **22** 206002
- [13] Kadomtseva A M *et al* 2010 *Low Temp. Phys.* **36** 511
- [14] Zvezdin A K, Krotov S S, Kadomtseva A M, Vorob'ev G P, Popov Yu F, Pyatakov A P, Bezmaternykh L N and Popova E A 2005 *JETP Lett.* **81** 272
- [15] Zvezdin A K, Vorob'ev G P, Kadomtseva A M, Popov Yu F, Pyatakov A P, Bezmaternykh L N, Kuvardin A V and Popova E A 2006 *JETP Lett.* **83** 509
- [16] Kadomtseva A M, Popov Yu F, Vorob'ev G P, Mukhin A A, Ivanov V Yu, Kuz'menko A M and Bezmaternykh L N 2008 *JETP Lett.* **87** 39
- [17] Zvezdin A K, Kadomtseva A M, Popov Yu F, Vorob'ev G P, Pyatakov A P, Ivanov V Yu, Kuz'menko A M, Mukhin A A, Bezmaternykh L N and Gudim I A 2009 *JETP* **109** 68
- [18] Joubert J C, White W B and Roy R J 1997 *J. Appl. Crystallogr.* **1** 318
- [19] Campa J A, Cascales C, Gutierrez-Puebla E, Monge M A, Rasines I and Ruiz-Valero C 1997 *Chem. Mater.* **9** 237
- [20] Klimin S A, Fausti D, Meetsma A, Bezmaternykh L N, Loosdrecht P H M and Palstra T T 2005 *Acta Crystallogr. B* **61** 481
- [21] Yukio H, Yoshihiro D, Kentaro I, Makoto W and Abdolali A 2003 *J. Solid State Chem.* **172** 438
- [22] Chukalina E P, Popova M N, Bezmaternykh L N and Gudim I A 2010 *Phys. Lett. A* **374** 1790
- [23] Popova M N 2009 *J. Magn. Magn. Mater.* **321** 716
- [24] Popova M N, Chukalina E P, Stanislavchuk T N and Bezmaternykh L N 2006 *J. Magn. Magn. Mater.* **300** e440
- [25] Chukalina E P, Stanislavchuk T N, Popova M N, Bezmaternykh L N and Gudim I A 2007 *Bull. Russ. Acad. Sci.: Phys.* **71** 1563
- [26] Stanislavchuk T N, Chukalina E P, Popova M N, Bezmaternykh L N and Gudim I A 2007 *Phys. Lett. A* **368** 408
- [27] Malakhovskii A V, Gnatchenko S L, Kachur L S, Piryatinskaya V G, Sukhachev A L and Temerov V L 2010 *Bull. Russ. Acad. Sci.: Phys.* **74** 721
Malakhovskii A V, Gnatchenko S L, Kachur L S, Piryatinskaya V G, Sukhachev A L and Temerov V L 2011 *Eur. Phys. J. B* **80** 1
- [28] Popova M N, Chukalina E P, Stanislavchuk T N, Malkin B Z, Antic-Fidancev E and Bezmaternykh L N 2007 *Phys. Rev. B* **75** 224435
- [29] Popova M N, Stanislavchuk T N, Malkin B Z and Bezmaternykh L N 2009 *Phys. Rev. Lett.* **102** 187403
- [30] Popova M N, Stanislavchuk T N, Malkin B Z and Bezmaternykh L N 2009 *Phys. Rev. B* **80** 195101
- [31] Bezmaternykh L N, Temerov V L, Gudim I A and Stolbovaya N A 2005 *Crystallogr. Rep.* **50** 97 (suppl. 1)
- [32] Dieke G H 1968 *Spectra and Energy Levels of Rare Earth Ions in Crystals*, ed H M Crosswhite and H Crosswhite (New York: Interscience Publishers)
- [33] Popova M N 2001 *Encyclopedia of Materials: Science and Technology* (Amsterdam: Elsevier) p 3786
- [34] Couwenberg I, Binnemans K, De Leebeek H and Göller-Walrand C 1998 *J. Alloys Compounds* **274** 157
- [35] Baraldi A, Buffagni E, Capelletti R, Mazzera M, Földvári I, Beregi E and Magnani N 2010 *IOP Conf. Ser.: Mater. Sci. Eng.* **15** 012034
- [36] Popova M N, Boldyrev K N, Petit P O, Viana B and Bezmaternykh L N 2008 *J. Phys.: Condens. Matter* **20** 455210
- [37] Boldyrev K, Popova M, Bezmaternykh L and Bettinelli M 2011 *Quantum Electron.* **41** 120
- [38] Carnall W T, Goodman G L, Rajnak K and Rana R S 1989 *J. Chem. Phys.* **90** 3443
- [39] Liu G K, Huang J, Cone R L and Jacquier B 1988 *Phys. Rev. B* **38** 11061
- [40] Levy P M 1964 *Phys. Rev.* **135** A155
- [41] Jorgensen C K and Judd B R 1964 *Mol. Phys.* **8** 280
- [42] Ritter C, Vorotynov A, Pankrats A, Petrakovskii G, Temerov V, Gudim I and Szymczak R 2010 *J. Phys.: Condens. Matter* **22** 206002
- [43] Kuzmenko A M, Mukhin A A, Ivanov V Yu, Kadomtseva A M, Lebedev S P and Bezmaternykh L N 2011 *JETP* **113** 113